
Article:

Joel, A.S., Wang, M., Ramshaw, C. et al. (2017) Modelling, simulation and analysis of intensified regenerator for solvent based carbon capture using rotating packed bed technology. Applied Energy, 203. pp. 11-25. ISSN: 0306-2619

https://doi.org/10.1016/j.apenergy.2017.05.157

Modelling, Simulation and Analysis of Intensified Regenerator for Solvent based Carbon Capture using Rotating Packed Bed Technology

Atuman S. Joel[a], Meihong Wang[b]*, Colin Ramshaw[b], Eni Oko[b]

[a]Process/Energy Systems Engineering Group, School of Engineering, University of Hull, HU6 7RX, UK
[b]Department of Chemical and Biological Engineering, University of Sheffield, S1 3JD, UK
*Corresponding author. Tel: +44(0) 1142 227160. ; Email address: Meihong.Wang@sheffield.ac.uk

ABSTRACT

Intensified regenerator/stripper using rotating packed bed (RPB) for regeneration of rich-MEA solvent in post-combustion CO_2 capture with chemical absorption process was studied through modelling and simulation in this paper. This is the first systematic study of RPB regenerator through modelling as there is no such publication in the open literature. Correlations for liquid and gas mass transfer coefficients, heat transfer coefficient, liquid hold-up, interfacial area and pressure drop which are suitable for RPB regenerator were written in visual FORTRAN as subroutines and then dynamically linked with Aspen Plus® rate-based model to replace the default mass and heat transfer correlations in the Aspen Plus®. The model now represents intensified regenerator/stripper. Model validation shows good agreement between model predictions and experimental data from literature. Process analyses were performed to investigate the effect of rotor speed on the regeneration efficiency and regeneration energy (including motor power). The rotor speed was varied from 200 to 1200 rpm, which was selected to cover the validation range of rotor speed. Impact of reboiler temperature on the rate of CO_2 stripping was also investigated. Effect of rich-MEA flow rate on regeneration energy and regeneration efficiency was studied. All the process analyses were done for wide range of MEA concentration (32.6 wt%, 50 wt% and 60 wt%). Comparative study between regenerator using packed column and intensified regenerator using RPB was performed and the study shows a size reduction of 9.691 times. This study indicates that RPB process has great potential in thermal regeneration application.

Keywords: *Post-combustion CO_2 capture, MEA solvent, Process Intensification (PI), Rotating Packed Bed (RPB), Process Modelling, Process simulation*

1 Introduction

1.1 *Background*

Environmental concern has posed many questions as to the impact of greenhouse gas to those changes currently noticed in world climate and the future dangers that will be expected if mitigation measures are not put in place. Combustion of coal and petroleum accounts for the majority of the anthropogenic CO_2 emissions. Petroleum is mostly used as a transportation fuel for vehicles while coal is used mostly for electricity generation, for instance about 85.5% of coal is used for electricity generation in 2011 in the UK [1]. Albo *et al.* [2] stated that among the greenhouse gases, CO_2 contributes to more than 60% of global warming. Statistics from World Metrological Organisation (WMO) showed the amount of CO_2 in the atmosphere reached 393.1 ppm in 2012. The WMO report also showed that the amount of CO_2 in the atmosphere has increased on average by 2 ppm per year for the past 10 years. Recent report by CO2-Earth [3] shows that as at 8 April 2017 CO_2 atmospheric concentration stood at 407.78 ppm, this increased atmospheric concentration of CO_2 affects the radiative balance of the earth surface [4].

In order to meet the set target of 50% emission reduction by 2050 as compared to the level of 1990 as proposed by Intergovernmental panel on climate change (IPCC) [5], carbon capture and storage (CCS) is an important option for that target to be achieved. The International Energy Agency (IEA) [6] identifies CCS as a significant and low-cost option in fighting climate change. The most matured CO_2 capture technology is post-combustion CO_2 capture (PCC) based on chemical absorption as reported in Mac Dowell *et al.* [7] which is also believed to be a low-risk technology and promising near-term option for large-scale CO_2 capture.

PCC for coal-fired power plants using conventional packed columns has been reported by many authors. Dugas [8] carried out pilot plant study of PCC in the context of fossil fuel-fired power plants. Lawal *et al.* [9-11] carried out dynamic modelling and process analysis of CO_2 absorption for PCC in coal-fired power plants. In all these studies, one of the identified challenges to the commercial roll-out of the technology has been the high capital and operating costs which has an unavoidable impact on electricity cost. Systematic study of aqueous monoethanolamine (MEA)-based CO_2 capture process looking at the techno-economic assessment of the MEA process and its improvements was reported by Li *et al*. [12]. Oh *et al*. [13] study energy minimization of MEA-based CO_2 capture process it was found that Flue gas splitting gives a significant reduction of energy consumption. Solvent performance comparison for a large scale pulverized coal power plant was reported by Sharifzadeh *et al.* [14]. Hanak *et al*. [15] reported efficiency improvements for the coal-fired power plant retrofit with CO_2 capture plant using chilled ammonia process showing efficiency penalty reduced to 8.7% Also Zhao *et al.* [16] using mixed solvent for 650 MW power plant reported that the net power efficiency penalty was reduced from 9.13% to 7.66%. Approaches such as heat integration, inter-cooling among others could reduce the operating cost slightly. However, they limit the plant flexibility and will make operation and control more difficult [17]. Process intensification (PI) has the potential to meet this challenge [18-20].

Study of intensified absorber was reported in Joel *et al* [21,22] and Agarwal *et al.* [23]. Joel *et al* [21] reported 12 times volume reduction for absorber if using RPB technology as compared to packed column. Results from Agarwal *et al.* [23] indicated 7 times volume reduction when using RPB as compared to conventional packed column. The study by Joel *et al.* [21] uses aqueous MEA solvent while Agarwal *et al.* [23] uses diethanolamine (DEA) as solvent. This is the main reason for the differences in size reduction since faster reaction rate means shorter residence time and slower reaction rate means longer residence time required for the same capture rate. Jassim *et al.* [24] and Cheng *et al.* [25] reported experimental studies on intensified regenerator using RPB. Zhao *et al*. [26] study the mass transfer performance of CO_2 capture in rotating packed bed and Chamchan *et al*. [27] compared RPB and PB absorber in pilot plant.

Figure 1 is a typical process flow diagram of an intensified regenerator using RPB for solvent regeneration. The flowsheet was used by Jassim *et al.* [24] and Cheng *et al.* [25] for experimental study. One of the operational benefits of using RPB is its ability to be operated at higher gas and/or liquid flow rates owing to the low tendency of flooding compared to that in the conventional packed bed [28]. Another benefit of using RPB is its better self-cleaning, avoidance of blocking in the system, and being unaffected by a moderate disturbance in its orientation [29].

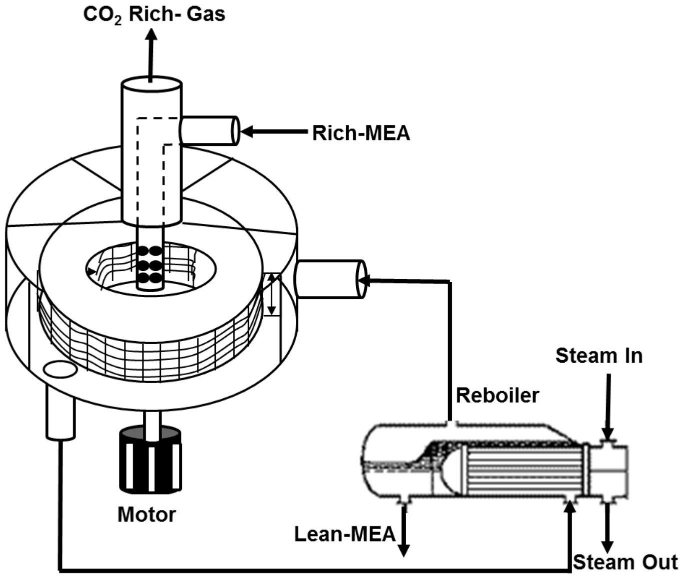

Figure 1 Schematic diagram of an RPB regenerator

Nomenclature

a	effective interfacial area (m^2/m^3)
a_i	activity of species *i* in a solution
a_t	total specific surface area of packing (m^2/m^3)
a_w	wetted area per unit volume (m^2/m^3)

a'_p	parameter for Chen et al. [24] and Chen [25] correlations for liquid and gas film mass transfer coefficients (= 3000 m^2/m^3)
c	width of wire mesh packing opening (mm)
C_i^l	concentration of component *i*
Cp_i	heat capacity for component *i*
d	wire diameter of wire mesh packing (mm)
D	column diameter (m)
D_G	diffusivity of gas (m^2/s)
D_L	diffusivity of liquid (m^2/s)
E_j	activation energy (kJ/mol)
d_p	packing size (m)
G	volumetric gas flow rate (m^3/s)
G^m	Gas molar flowrate (kmol/s)
g_c	gravitational acceleration or acceleration due to centrifugal field (m^2/s)
g_o	characteristic acceleration value (100 m^2/s)
H	height of packing (m)
h_G	gas phase specific molar enthalpy (J/kmol)
h_L	liquid phase specific molar enthalpy (J/kmol)
$h_{g/l}$	interfacial heat transfer coefficient (W/m^2 K)
ΔH_r	heat of desorption of CO_2 (*J/kmol*)
ΔH_{vap}	heat of vaporisation of H_2O (*J/kmol*)
k_G	gas film mass transfer coefficient (m/s)
K_G^a	overall mass transfer coefficient (1/s)
k_j^o	pre-exponential factor ($kmol/m^3.s$)
k_L	liquid film mass transfer coefficient (m/s)
L	Liquid mass flowrate per tangential area ($kg/m^2/s$)
L^m	Liquid molar flowrate (*kmol/s*)
MEA	Monoethanolamine
N_i	molar fluxes for component *i (kmol/m^2 s)*
P_{motor}	motor power (kilowatts)
Q_L	volumetric flow rate of liquid (m^3/s)
r	radial position (m)
R_c	ideal gas constant (J $kmol^{-1}$ K^{-1})
r_j	reaction rate for reaction *j*
rxn_i	reaction rate of component *i*, (*$kmol/m^3/s$*)

r_i	inner radius of the RPB (m)
r_o	outer radius of the RPB (m)
r_s	radius of the stationary housing of the RPB (m)
T	temperature (K)
$\mathrm{t_{res}}$	residence time (s)
u_l	superficial liquid velocity (m/s)
u_g	superficial gas velocity (m/s)
U_o	characteristic superficial liquid velocity (1cm/s)
V	volume of the liquid films in the RPB (m^3)
V_i	volume inside the inner radius of the RPB = $\pi r_i^2 Z$ (m^3)
V_o	volume between the outer radius of the bed and the stationary housing = $\pi(r_s^2 - r_0^2)Z$ (m^3)
V_t	total volume of the RPB = $\pi r_s^2 Z$ (m^3)
x_i	Component molar fraction in liquid phase
y_i	Component molar fraction in gas phase
$y_{CO_{2,in}}$	mole fraction of CO_2 in inlet gas stream
$y_{CO_{2,out}}$	mole fraction of CO_2 in outlet gas stream
Z	axial height of the RPB (m)

Greek letters

α_{ij}	reaction order of species *i* in reaction *j*
ε	porosity of packing, m^3/m^3
$\in_L$	liquid holdup (m^3/m^3)
μ	viscosity (Pa.s)
ρ_L	liquid density (kg/m^3)
ρ_G	gas density (kg/m^3)
σ	liquid surface tension (N/m)
σ_c	critical surface tension (N/m)
σ_w	surface tension of water (N/m)
v_L	kinematic liquid viscosity (m^2/s)
v_G	kinematic gas viscosity (m^2/s)
ω	angular velocity (rad/s)

Dimensionless groups

Fr_L	liquid Froude number $(u_l^2 a_t / g_c)$
Gr_G	gas Grashof number $\left(d_p^3 g_c / v_G^2\right)$

Gr_L	liquid Grashof number $\left(d_p^3 g_c / \nu_L^2\right)$
Re_G	gas Reynolds number $(u_g / a_t \nu_G)$
Re_L	liquid Reynolds number $(u_l / a_t \nu_L)$
Sc_L	liquid Schmidt number (ν_L / D_L)
We_L	liquid Webber number $(u_l^2 \rho_L / a_t \sigma)$
φ	theoretical probability of liquid uncaptured by fibers $(c^2/(d+c)^2)$)

1.2 *Motivation*

Over 8,000 tonnes of CO_2 per day will be released from a typical 500 MWe advanced supercritical coal fired power plant operating at 46% overall net power plant efficiency (LHV basis) [30]. This huge volume of flue gas will require big column size. Lawal *et al.* [9] reported dynamic modelling study of a 500 MWe sub-critical coal-fired power plant using the packed column (i.e. conventional technology). From the study, one regenerator of 17m in packing height and 9 m in diameter will be needed for regeneration of rich-MEA solvent. This huge packed column will mean higher capital and operating costs, therefore a technological option leading to smaller equipment size is very important. Kothandaraman *et al.* [31] reported that in conventional packed tower majority (approximately 62%) of the energy consumed during the CO_2 capture process was used for the solvent regeneration, therefore it is necessary to look for technological options that will reduce this energy requirement.

1.3 *Novel contributions of the paper*

This is the first systematic study on RPB regenerator through modelling as there is no such publication in the open literature. There are four novel aspects in this paper: (a) A new first principle model for intensified regenerator using RPB was developed which was implemented in Aspen Plus® rate-based model by replacing different correlations for mass transfer, interfacial area and liquid hold-up. Steady state validation of the intensified regenerator is performed using experimental data from Jassim *et al.* [24] and Cheng *et al.* [25]. (b) Process analysis of the intensified regenerator involving different process scenarios were carried out to gain insights for process design and operation. These process scenarios are: (i) the impact of rotational speed on the regeneration efficiency and regeneration energy at fixed intensified regenerator size and rich-MEA flow rate was studied; (ii) the effect of rich-MEA solvent flow rate on the regeneration efficiency and regeneration energy was explored; (iii) the effect of reboiler temperature on regeneration efficiency and regeneration energy was explored. (c) Comparative study was performed between intensified regenerator using RPB and conventional regenerator using packed bed. It was found that there is 9.69 times reduction in size under the same conditions which means decrease in equipment capital cost. (d) The study were done over wide range of MEA concentrations (32.6 wt%, 50 wt% and 60 wt%) and the energy consumption per ton of CO_2 is within the range of conventional packed column.

2 Model Development

Model for intensified regenerator using RPB does not exist in any commercially available model library (including Aspen Plus®). To model intensified regenerator using RPB, the default mass/heat transfer correlations in the Aspen Plus® rate-based model have to be replaced with subroutines written in Intel® visual FORTRAN. The new model now represents an intensified regenerator using RPB. The new steady state model is still developed based on two-film theory Joel *et al.* [21]. The correlations include: liquid phase mass transfer coefficient given by Chen *et al.* [32], gas-phase mass transfer coefficient given by Chen [33], interfacial area correlation estimated by Luo *et al.* [34] and liquid hold-up correlation given by Burns *et al.* [35]. Dry pressure drop expression was used since it accounts in an additive manner of the drag and centrifugal forces, the gas-solid slip and radial acceleration effect [36].

2.1 *Main governing equations*

The main governing equations include material and energy balance equations. Momentum balance is reflected in the pressure drop relation presented in Section 2.7.

2.1.1 Gas and liquid phase material balances

Assuming steady state conditions, material balances for gas and liquid phase in the RPB is described by Equations 1 and 2. Due to flow directions in RPB, the equations are based on numerical discretisation in the radial direction. Also, the term $2\pi rZ$ is described preferably as tangential area to differentiate it from cross sectional area as it varies from section to section along the radial direction.

Material balances for gas phase:

$$0 = \frac{1}{2\pi rZ}\frac{\partial(G^m y_i)}{\partial r} - aN_i \qquad (1)$$

Material balances for liquid phase:

$$0 = -\frac{1}{2\pi rZ}\frac{\partial(L^m x_i)}{\partial r} + aN_i + \in_L rxn_i \qquad (2)$$

The equation includes component molar flow balances (represented by the derivative terms) across each radial segment per tangential area, interfacial molar fluxes (aN_i) and liquid phase reaction rate ($\in_L rxn_i$). By this, reactions are deemed to occur only in the liquid phase and ionic components therefore only exist in the liquid phase.

2.1.2 Gas and liquid phase energy balances

Energy balances for gas and liquid phase is given by Equations 3 and 4 respectively [37]

Energy balances for gas phase:

$$0 = \frac{1}{2\pi r Z}\frac{\partial (G^m h_G)}{\partial r} - a h_{\frac{g}{l}}\left(T_l - T_g\right) - Q_G^{Loss} \qquad (3)$$

Energy balances for liquid phase:

$$0 = -\frac{1}{2\pi r Z}\frac{\partial (L^m h_L)}{\partial r} - a\left(h_{g/l}\left(T_l - T_g\right) - \Delta H_r N_{CO_2} - \Delta H_{vap} N_{H_2O}\right) - Q_L^{Loss} \qquad (4)$$

The equations include interfacial heat transfer, $h_{g/l}(T_l - T_g)$, heat released due to CO_2 desorption from the loaded MEA solvent, $\Delta H_r N_{CO_2}$ and heat released or absorbed due to H_2O condensation or vaporization, $\Delta H_{vap} N_{H_2O}$, [17]. Due to the relatively higher temperature of the stripper compared to ambient condition, heat losses (Q_G^{Loss} and Q_L^{Loss}) are also taken into account.

2.2 *Physical property*

Electrolyte Non-Random-Two-Liquid (ElecNRTL) activity coefficient model in Aspen Plus® was used to describe the vapour–liquid equilibrium, the chemical equilibrium and the physical properties of the system. The equilibrium constants for reactions 5-9 are calculated from the standard Gibbs free energy change, the equilibrium reactions are assumed to occur in the liquid film and kinetic reactions equations and parameters are obtained from AspenTech [38]. The electrolyte solution chemistry which is used in property calculation is modelled with chemistry model and all the ionic reactions are assumed to be in chemical equilibrium as shown in Equations 5-9 [38].

Equilibrium $\quad 2H_2O \leftrightarrow H_3O^+ + OH^-$ (5)

Equilibrium $\quad CO_2 + 2H_2O \leftrightarrow H_3O^+ + HCO_3^-$ (6)

Equilibrium $\quad HCO_3^- + H_2O \leftrightarrow H_3O^+ + CO_3^{2-}$ (7)

Equilibrium $\quad MEAH^+ + H_2O \leftrightarrow MEA + H_3O^+$ (8)

Equilibrium $\quad MEACOO^- + H_2O \leftrightarrow MEA + HCO_3^-$ (9)

Kinetic reactions used for the intensified stripping calculation is specified by Equations 10-13 in the reaction part of the regenerator model in the Aspen Plus.

Kinetic $\quad CO_2 + OH^- \rightarrow HCO_3^-$ (10)

Kinetic $\quad HCO_3^- \rightarrow CO_2 + OH^-$ (11)

Kinetic $\quad MEA + CO_2 + H_2O \rightarrow MEACOO^- + H_3O^+$ (12)

Kinetic $\mathrm{MEACOO^- + H_3O^+ \rightarrow MEA + CO_2 + H_2O}$ (13)

Power law expression Equation 14 is used for the rate-controlled reactions. The kinetic parameters for reactions in Equations 10-13 were listed in Table 1

$$r_j = k_j^o exp\left(-\frac{E_j}{R_c}\left[\frac{1}{T} - \frac{1}{298.15}\right]\right) \prod_{i=1}^{N} a_i^{\alpha_{ij}} \tag{14}$$

Table 1 Constants for power law expressions for the absorption of CO_2 by MEA [39]

Reaction No.	k_j^o (kmol/m^3.s)	E_j, kJ/mol
10	1.33e+17	55.38
11	6.63e+16	107.24
12	3.02e+14	41.2
13	6.56e+27	95.24

2.3 *Liquid phase mass transfer coefficient*

An expression was introduced by Tung and Mah [40] based on penetration theory to describe the liquid mass transfer behaviour in the RPB.

$$\frac{k_L d_p}{D_L} = 0.919\left(\frac{a_t}{a}\right)^{1/3} Sc_L^{1/2} Re_L^{2/3} Gr_L^{1/6} \tag{15}$$

This correlation was developed without considering the Coriolis force or the effect of the packing geometry. This is why there is a need for an alternative correlation for liquid phase mass transfer coefficient.

Chen *et al.* [32] developed liquid phase mass transfer correlation considering the end effect and packing geometry. The correlation was found to be valid for different sizes of the RPBs and for viscous Newtonian and non-Newtonian fluids. Because of these advantages, Equation 16 is selected for calculating the liquid phase mass transfer coefficient, and also findings from Joel *et al.* [22] suggested the use of Equation 16 because of it smaller error prediction.

$$\frac{k_L a d_p}{D_L a_t}\left(1 - 0.93\frac{V_o}{V_t} - 1.13\frac{V_i}{V_t}\right) = 0.35 Sc_L^{0.5} Re_L^{0.17} Gr_L^{0.3} We_L^{0.3} \left(\frac{a_t}{a_p'}\right)^{-0.5} \left(\frac{\sigma_c}{\sigma_w}\right)^{0.14} \tag{16}$$

2.4 *Gas phase mass transfer coefficient*

Onda *et al.* [41] correlation for calculating gas-side mass transfer coefficient (Equation 17) was developed for conventional packed column. Sandilya *et al.* [42] suggested that the gas rotates like a solid body in the rotor because of the drag force caused by the packing, which means that gas-side mass transfer coefficient should be similar to that in a conventional packed column, but the end effect and packing effect were not considered, this makes the authors to select Equation 18 proposed by Chen [33] instead of Equation 17.

$$k_G = 2.0(a_t D_G) Re_G^{0.7} Sc_G^{1/3} \left(a_t d_p\right)^{-2} \tag{17}$$

Chen [33] presented local gas-side mass transfer coefficient correlation using two-film theory for RPB. Equation 18 for calculating the gas phase mass transfer coefficient was used in the model because it accounts for the effect of rotation of the RPB.

$$\frac{k_G a}{D_G a_t^2}\left(1 - 0.9\frac{V_o}{V_t}\right) = 0.023 Re_G^{1.13} Re_L^{0.14} Gr_G^{0.31} We_L^{0.07} \left(\frac{a_t}{a_p'}\right)^{1.4} \tag{18}$$

2.5 *Total gas-liquid interfacial area*

Total gas-liquid interfacial area correlation for conventional packed column was developed by Onda *et al.* [41] as shown in Equation 19. It can be modified to account for the effect of rotation of the bed but because it is not originally designed for RPB and also it was not designed for different types of packing, Equation 20 developed by Luo *et al* [34] was selected.

$$\frac{a}{a_t} = 1 - exp\left[-1.45\left(\frac{\sigma_c}{\sigma}\right)^{0.75} Re_L^{0.1} We_L^{0.2} Fr_L^{-0.05}\right] \tag{19}$$

Luo *et al.* [34] studied gas-liquid effective interfacial area in an RPB considering different types of packing, also taking into account the effect of fibre diameter and opening of the wire mesh.

$$\frac{a}{a_t} = 66510 Re_L^{-1.41} Fr_L^{-0.12} We_L^{1.21} \varphi^{-0.74} \tag{20}$$

2.6 *Liquid hold-up*

Liquid holdup correlation given by Burns *et al.* [35] was used. The correlation is based on data obtained through measurement of electrical resistance across sections of an RPB. The study showed that the liquid hold-up is approximately inversely proportional to the local packing radius and is largely independent of gas flow up to the flooding point and also liquid viscosity has only a weak influence on hold-up [35].

$$\in_L = 0.039\left(\frac{g_c}{g_o}\right)^{-0.5}\left(\frac{u_l}{U_o}\right)^{0.6}\left(\frac{v_L}{v_o}\right)^{0.22} \tag{21}$$

$$g_o = 100\, m\, s^{-2}, \quad U_o = 1\, cm\, s^{-1}, \quad v_o = 1\, cS = 10^{-6}\, m^2\, s^{-1}$$

$$u_l = \frac{Q_L}{2\pi r Z} \tag{22}$$

2.7 *Dry pressure drop expression*

Semi-empirical dry pressure drop expression was given by Llerena-Chavez and Larachi [36]. The correlation was developed based on Ergun-type semi-empirical relationships in which the gas-slip and radial acceleration effects, the laminar and inertial drag effects and the centrifugal effect were aggregated additively to form the pressure drops correlation in the RPB [36].

$$\Delta P_{Packed\ bed} = \frac{150(1-\varepsilon)^2\mu}{d^2\varepsilon^3}\left(\frac{G}{2\pi Z}\right)\ln\frac{r_o}{r_i} + \frac{1.75(1-\varepsilon)\rho}{d\varepsilon^3}\left(\frac{G}{2\pi Z}\right)^2\left(\frac{1}{r_i}-\frac{1}{r_o}\right)$$

$$+\frac{1}{2}\rho\omega^2(r_o^2 - r_i^2) + F_c \tag{23}$$

where F_c is a corrective function given as:

$$F_c = \varepsilon(a - G + (b + \omega^c)G^2) \tag{24}$$

a, b, and c are fitting parameters given as:

$$a = -0.08\ m^3/s \qquad b = 2000(rpm)^c \qquad c = 1.22$$

2.8 *Power consumption by RPB stripper motor*

The amount of power consumed by motor for rotating RPB absorber and stripper is calculated using the correlation proposed by Singh *et al.* [43]. The correlation was used to account for all the frictional losses and also the power required for accelerating the liquid entering the packing bed to the rotational speed at the outer radius. It is important to note that frictional losses are highly dependent upon the design of the machine and cannot be predicted without advance knowledge of the design (i.e., type of bearings, direct or pulley drive, etc.) [43].

$$P_{motor} = 1.2 + 1.1 \times 10^{-3}\rho_L r_o^2 \omega^2 Q_L \tag{25}$$

2.9 *Modelling and simulation methodology*

The procedure used in this paper for modelling and simulation of the RPB is shown in **Figure 2** and summary of the model parameters and correlations were presented in **Table 2**

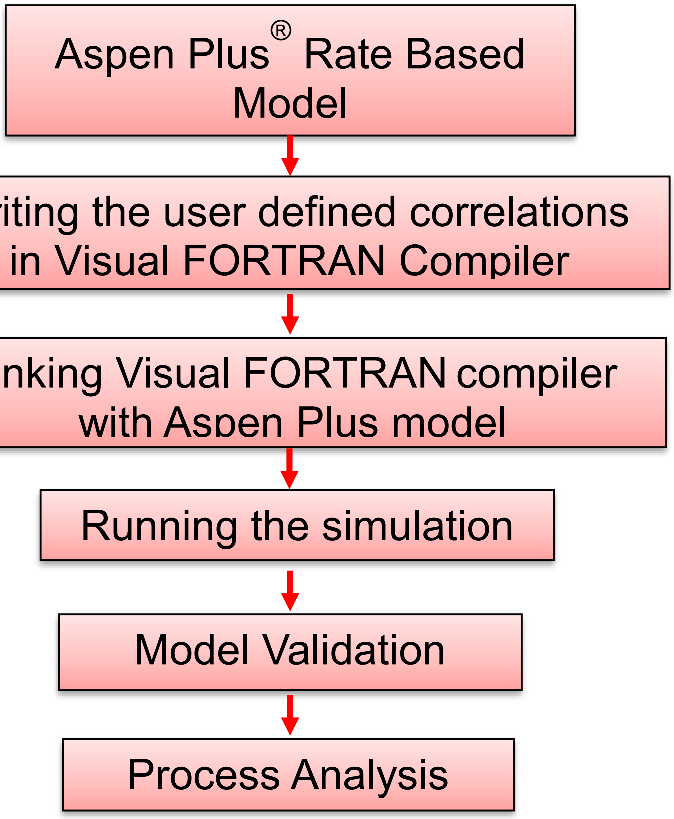

Figure 2 Methodology used in this paper [21,22]

Table 2 Summary of model parameters

Parameters	Correlations or values	
	Jassim *et al*	Cheng *et al*
Model geometry		
r_i (m)	0.156	0.076
r_o (m)	0.398	0.160
h (m)	0.025	0.020
surface area of the packing per unit volume of the bed (m^2/m^3)	2132	803
Liquid phase mass transfer coefficient	See Equation 16	
Gas phase mass transfer coefficient	See Equation 18	
Total gas-liquid interfacial area	See Equation 20	
Liquid holdup	See Equation 21	
Dry pressure drop expression	See Equation 23	
Motor power	See Equation 25	

3 Model Validation

3.1 *Model validation using experimental data from Jassim et al. [24]*

The experimental data used for the model validation was obtained from Jassim *et al.* [24]. From their experiments, rich-MEA concentration of 32.9 wt%, 35.7 wt%, 30.8 wt%, 57.4 wt% and 52 wt% were selected for the validation study. The equipment specifications and process input conditions for the validation study are shown in **Tables 3 and 4.** The study was done under two different rotor speeds 800 rpm and 1000 rpm.

Table 3 RPB stripper packing specifications used by Jassim et al. [24]

Description	**Value**
RPB outer diameter	0.398 m
RPB inner diameter	0.156 m
RPB axial depth	0.025 m
Packing specific surface area	2132 m^2/m^3
Packing porosity	0.76

Table 4 Input process conditions for Run 1 to Run 5 [24]

	Runs				
	Run 1	Run 2	Run 3	Run 4	Run 5
Rotor speed (RPM)	800	800	800	1000	1000
Rich-MEA temperature (°C)	67.100	69.000	70.000	57.200	58.400
Rich-MEA pressure (kPa)	101.325	101.325	101.325	101.325	101.325
Rich-MEA flow rate (kg/s)	0.200	0.200	0.400	0.400	0.200
Rich-MEA composition (wt. %)					
H_2O	58.116	54.013	61.536	25.142	32.895
CO_2	8.984	10.287	7.664	17.458	15.105
MEA	32.900	35.700	30.800	57.400	52.000
Rich-MEA CO_2 loading (mol CO_2 /mol MEA)	0.3790	0.3999	0.3454	0.4221	0.4030

Table 5 Simulation results compared to experimental data [24] for Run 1 to Run 5

	Runs				
	Run 1	Run 2	Run 3	Run 4	Run 5
Rotor speed (RPM)	800	800	800	1000	1000
Experimental measurement					
Lean-MEA CO_2 loading (mol/mol)	0.321	0.329	0.329	0.403	0.334
Model prediction					
Lean-MEA CO_2 loading (mol/mol)	0.316	0.295	0.298	0.355	0.320
Relative error (%)	1.558	10.334	9.422	11.911	4.192

Model validation is shown in **Table 5** which gives percentage error prediction of not more than 12 % on the lean-MEA CO_2 loading. The lean-MEA CO_2 loading was evaluated on mole basis as shown in Equation 26.

$$\text{Loading} = \frac{\text{Moles of all } \mathrm{CO_2} \text{ carrying species}}{\text{Moles of all MEA carrying species}} = \frac{[CO_2] + [HCO_3^-] + [CO_3^{2-}] + [MEACOO^-]}{[MEA] + [MEA^+] + [MEACOO^-]} \quad (26)$$

Jassim *et al.* [24] didn’t include experimental results on reboiler duty, therefore the authors cannot compare model predictions with experimental tests.

3.2 *Model validation based on experimental data from Cheng et al. [25]*

Cheng et al [25] carried out experimental study on the thermal regeneration of alkanolamines solutions in a RPB using 30 wt% MEA aqueous solution loaded with CO_2 and a CO_2 - loaded aqueous solution consisting of 20 wt% diethylenetriamine and 10 wt% piperazine. For the purpose of this study, experimental data with 30 wt% MEA aqueous solution was used for model validation. RPB stripper specifications and process input conditions for the model are shown in **Tables 6 and 7**.

Table 6 RPB stripper packing specifications used by Cheng et al [25]

Description	**Value**
RPB outer diameter	0.160 m
RPB inner diameter	0.076 m
RPB axial depth	0.020 m
Packing specific surface area	803 m^2/m^3
Packing porosity	0.960

Table 7 Input process conditions for different reboiler temperature [25]

Variable	Reboiler Temperature		
	105 °C	**115 °C**	**120 °C**
Rotor speed (RPM)	900	900	900
Rich-MEA temperature (°C)	96.6	97	97
Rich-MEA pressure (kPa)	202.65	202.65	202.65
Rich-MEA flow rate (mL/min)	400	400	400
Rich-MEA CO_2 loading (mol CO_2/mol MEA)	0.484	0.484	0.484

Table 8 Simulation results compared to experimental data [25]

Variable		**Reboiler Temperature (°C)**		
		105	**115**	**120**
Lean Loading (mol CO_2/mol MEA)	Experimental measurement	0.418	0.340	0.271
	Model prediction	0.423	0.367	0.289
	Relative error (%)	**1.132**	**8.054**	**6.848**
Reboiler duty (kW)	Experimental measurement	0.620	0.900	1.240
	Model prediction	0.629	0.989	1.383
	Relative error (%)	**1.487**	**9.951**	**11.498**

Model results compared with the experimental data from Cheng *et al*. [25] shown in **Table 8** indicates a good agreement with relative error on lean loading of less than 9% and reboiler duty percentage error of less than 12% for different reboiler temperatures.

In summary, the model has predicted all experimental data reasonably well with not more than 12% error prediction, the model developed can then be used to carry out process analysis in order to study the system behaviour when there is a change in some variables.

4 Process Analysis

With the validated models, we carried out process analysis to explore the effect of rich-MEA flow rate, rotor speed and reboiler temperature on (a) the regeneration efficiency calculated based on loading (Equation 27) and calculated based on amount of CO_2 in rich-MEA and lean-MEA solvent (Equation 28), (b) the regeneration energy (with and without motor power) expressed in Equations 29 and 30 respectively. But the electricity power consumed by motor is high grade while the steam power in the reboiler is a low grade, therefore for the two powers to be comparable, efficiency loss needs to be accounted for by multiplying the motor power with 2.5 (i.e. assuming 40% thermal efficiency in converting thermal heat into electricity. The reason is that solvent-based carbon capture can be used in different scenarios such as coal-fired subcritical power plants, coal-fired supercritical power plants, gas-fired power plants and other industrial manufacturing plants. 40% is a good assumption for these different scenarios). Equations 31 and 32 were used to estimate the solvent residence time in the RPB with the assumption that wetted area per unit volume is equal to specific surface area of the packing [44]. The RPB stripper used for the process analysis has the following packing geometry: outer radius = 0.371 m; inner radius = 0.152 m; axial depth of packing = 0.167 m; packing void fraction = 0.76; packing specific surface area = 2,132 m^2/m^3.

$$\text{Regeneration eff. 1} = \left(\frac{\text{Rich CO}_2\text{ loading} - \text{Lean CO}_2\text{ loading}}{\text{Rich CO}_2\text{ loading}}\right) \times 100 \qquad (27)$$

$$\text{Regeneration eff. 2} = \left(\frac{\text{Amount of CO}_2\text{ in Rich} - \text{Amount of CO}_2\text{ in Lean}}{\text{Amount of CO}_2\text{ in Rich}}\right) \times 100 \qquad (28)$$

$$\text{Regeneration energy (without motor power)} = \frac{\text{Reboiler duty}}{\text{Mass of CO}_2\text{ desorbed}} \qquad (29)$$

$$\text{Regeneration energy (with motor power)} = \frac{(\text{Reboiler duty} + P_{motor} \times 2.5)}{\text{Mass of CO}_2\text{ desorbed}} \qquad (30)$$

$$\text{Residence time } (\mathrm{t_{res}}) = \frac{V}{Q_L} \qquad (31)$$

Where

$$V = \left(\frac{3v_L Q_L}{2\pi Z a_w \omega^2}\right)^{1/3} (a_w 2\pi Z)\left[r_o^{4/3} - r_i^{4/3}\right] \qquad (32)$$

Q_L = liquid volumetric flowrate (m^3/s)

4.1 *Effect of rich solvent flow rate on regeneration efficiency and energy*

4.1.1 Justification for case study

Rich-MEA solvent flow rate not only has influence on the amount of CO_2 that will be stripped off from the regenerator, but also has relationship with the reboiler duty. Therefore study on the right quantity of rich-MEA solvent coming into the regenerator of fixed or given size is necessary.

4.1.2 Setup of the case study

For this study, the process input conditions are shown in Table **9** with the rich-MEA flow rate varying from 0.2 kg/s to 0.8 kg/s. Here the rich-MEA loading is kept constant (i.e. 0.482 mol CO_2/mol MEA). Also in this study lean-MEA loading and reboiler temperature are the two outputs parameters that were maintained at 0.3178 mol CO_2/mol MEA and 120 °C respectively. Reboiler temperature is maintained at 120 °C by controlling the back pressure regulator to the stripper.

Table 9 Process inputs

Variable	**Case 1**	**Case 2**	**Case 3**
Rich-MEA temperature (°C)	104	104	104
Rich-MEA pressure (kPa)	202.650	202.650	202.650
Rich-MEA flow rate (kg/s)	0.2 – 0.8	0.2 – 0.8	0.2 – 0.8
Rich-MEA composition (wt. %)			
H_2O	56.072	32.027	18.559
CO_2	11.328	17.530	21.010
MEA	32.600	50.443	60.431
Rich loading (mol CO_2/mol MEA)	0.482	0.482	0.482
Reboiler temperature (°C)	120	120	120
Rotor speed (RPM)	1000	1000	1000

4.1.3 Results and discussion

Figure 3a (using Equation 27) **and Figure 3b** (using Equation 28) show a constant regeneration efficiency as the rich-MEA flow rate increases, this is because the rich-MEA loading is the same for all the cases and the lean-MEA loading which is one of the output is controlled at the same value of 0.3178 mol/mol. **Figure 4a** presents the amount of CO_2 strip-off from the stripper as the rich-MEA flow rate increases. The graph shows an increase in the amount of CO_2 desorbed as the rich-MEA flow rate increases. This is attributed to increase in droplet flow regime. As liquid flowrate increases, the liquid breaks up more readily as they enter the rotating packing forming more droplets due to their higher velocity. Studies by Chambers and Walls [45] already showed that droplet flow regime in RPBs generally favours better mass transfer performance than the film flow regime. It is not surprising then that CO_2 desorption rate noticeably increases (**Figure 4a**) as liquid flowrate increases. **Figure 4a** also shows that higher MEA concentration gives higher CO_2 desorption rate. This is due to their higher loading capacity, which means the amount of CO_2 absorbed is more. Therefore, under similar conditions then, desorption rate from more concentrated MEA solution is expected to be more.

Figure 4b shows firstly that the residence time decreases with increasing liquid flowrate. To understand this, referring to Equations 31 and 32, it is seen that the residence time can be related to flowrate as follows (assuming other parameters in Equations 31 and 32 remain constant):

$$\mathrm{t_{res}} = KQ_L^{-\frac{2}{3}} \tag{33}$$

With K (= constant), this simply shows that increasing flowrate will result to lower residence time. In physical terms, this can be further explained by acknowledging that liquid velocity increases with flowrate. Higher liquid velocity means that delay within the system is less and this ultimately means lower residence time.

The other result shown in **Figure 4b** is increase in residence time as MEA solution concentration increases. This is due to increase in solution density (i.e. 1062.784 kg/m^3 for 32.6 wt%, 1162.062 kg/m^3 for 50.443 wt%, 1209.465 kg/m^3 for 60.431 wt%) and viscosity (i.e. 0.000681235 N.s/m^2 for 32.6 wt%, 0.000990415 N.s/m^2 for 50.443 wt%, 0.00125367 N.s/m^2 for 60.431 wt%).

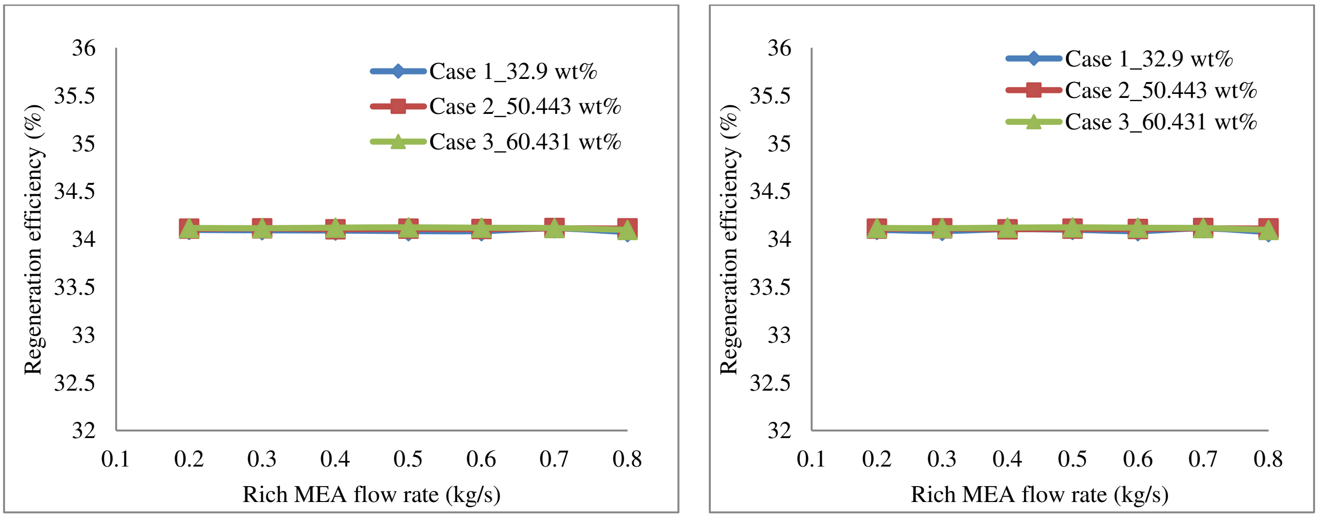

a b

Figure 3 Effect of rich-MEA flow rate on regeneration efficiency (a) using Equation 27 (b) using Equation 28

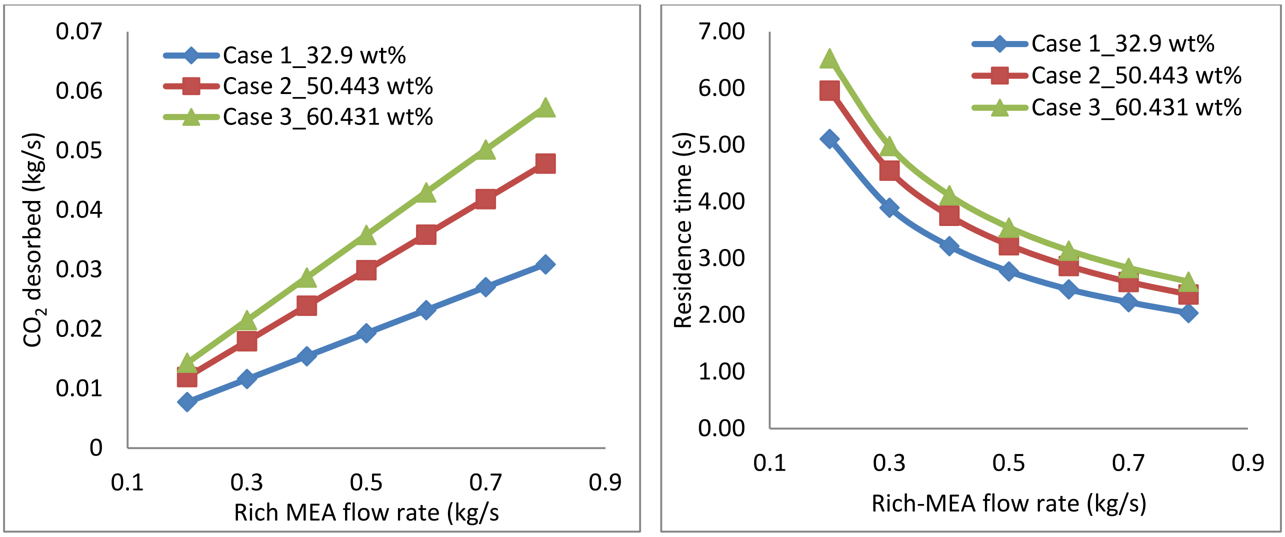

a b

Figure 4 Effect of rich-MEA flow rate on (a) CO_2 desorbed (b) Residence time

It can be observed from **Figure 5a,b** that the regeneration energy increases with increase in rich-MEA flow rate for Cases 2 and 3 (with and without motor power). For Case 1 (without motor energy) the regeneration energy is fairly constant as the rich-MEA flowrate increases as shown in **Figure 5a.** This is because the percentage increase in the reboiler duty shown in **Figure 6** is same as the percentage in CO_2 desorbed (**Figure 4a)** (i.e. 75.103% increase in reboiler duty and 74.973% increase in amount of CO_2 desorbed for Case 1) while for Case 2 there is 77.383% increase in reboiler duty and 75.003% increase in amount of CO_2 desorbed and Case 3 has 80.703% increase in reboiler duty, 74.986% increase in amount of CO_2 desorbed. The lowest regeneration energy obtained from the study is at flow rate of 0.2 kg/s rich-MEA. For Case 3 the regeneration energy is 5.17 GJ/ton CO_2 (without motor energy) and 5.44 GJ/ton CO_2 (with motor energy). The highest regeneration energy for Case 2 is at rich-MEA flow rate of 0.8 kg/s and the regeneration energy is 5.17 GJ/ton CO_2 (without motor energy) and 5.31 GJ/ton CO_2 (with motor energy). For Case 1 (with motor power) regeneration energy decreases with increase in rich-MEA flow.

The percentage increase in regeneration energy (i.e. including motor energy) when rich-MEA flowrate increases from 0.2 kg/s to 0.8 kg/s is 5.74% and 20.18% for Cases 2 and 3 respectively, while for Case 1 the regeneration energy decreases by 5.72%.

Looking at **Figures 5a,b and 6**, one may wonder why higher MEA concentration solvent is preferred for the RPB technology when the energy consumption is higher. It should be noted that here it is for stripper only. For a closed loop process including RPB Absorber and RPB stripper, the recycling solvent flowrate would be much lower for higher concentration solvent for the same capture efficiency in the absorber. Thus the energy consumption will be lower.

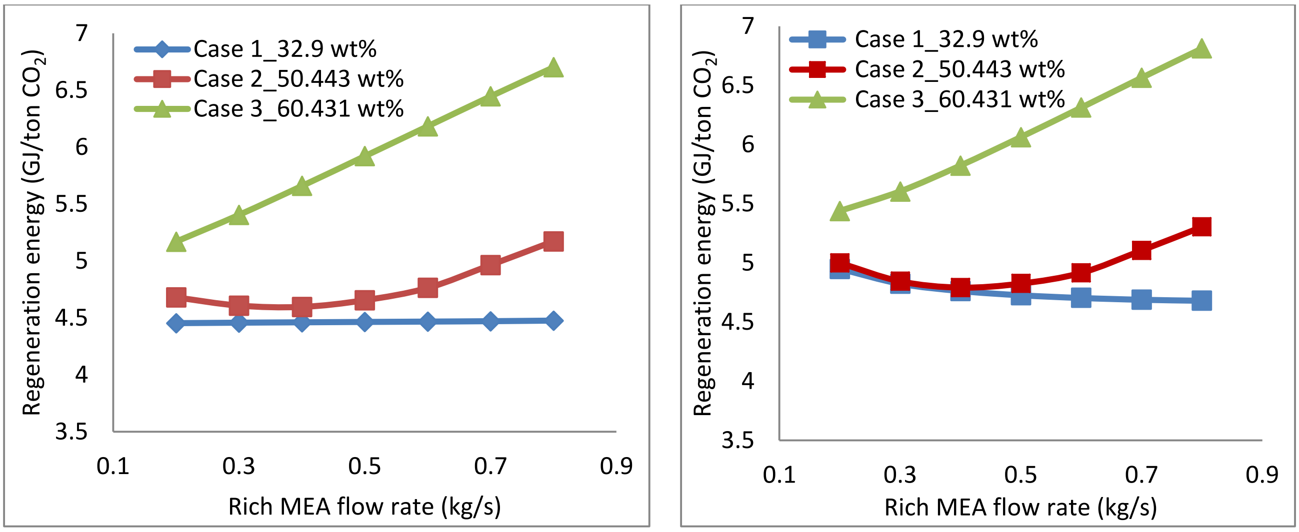

a b

Figure 5 Effect of rich-MEA flow rate on regeneration energy (a) without motor energy (b) with motor energy

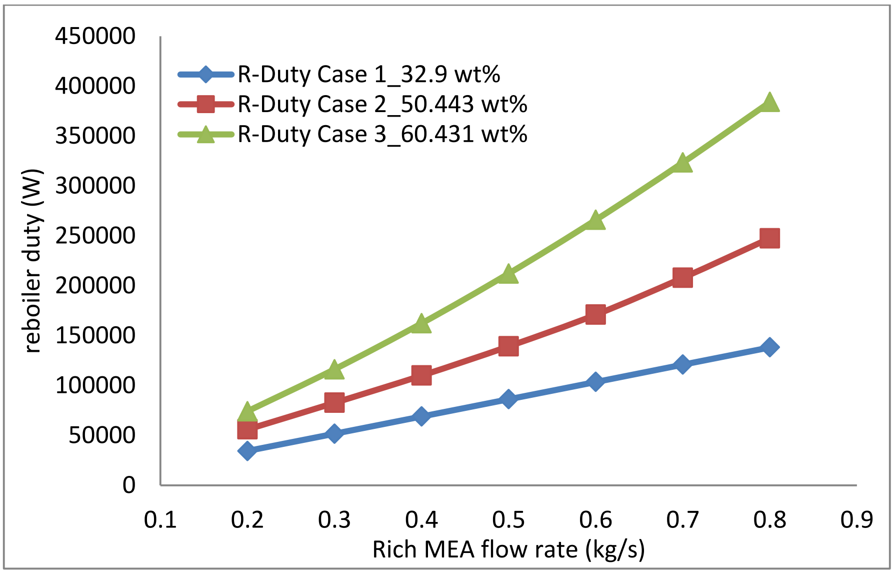

Figure 6 Effect of rich-MEA flow rate on reboiler duty

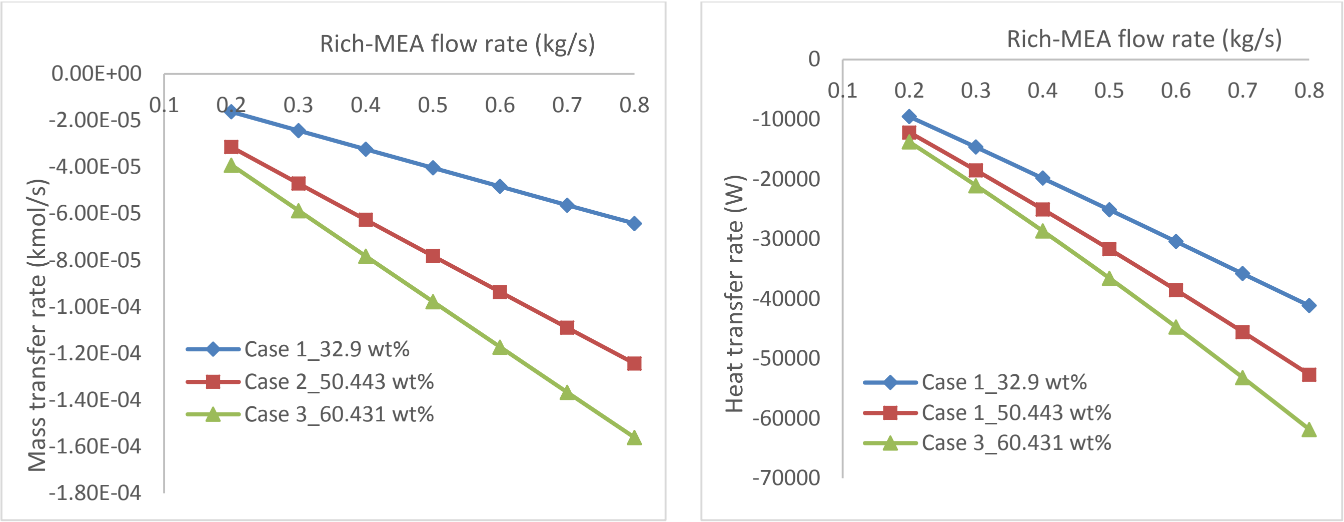

a

b

Figure 7 Effect of Rich-MEA flow rate on (a) mass transfer rate (b) heat transfer rate

Figure 7a shows how the CO_2 mass transfer rate increases as the rich-MEA flow rate increases. Mass transfer is generally defined as transfer from either vapour to liquid or liquid to vapour. Here CO_2 is transferred from liquid to vapour, therefore negative sign appears. **Figure 7a** shows higher mass transfer rate for high MEA concentration this is because more CO_2 has been dissolve in it, therefore the rate of CO_2 desorbed will be higher than the lower MEA concentration. In **Figure 7b** heat transfer rate increases with increase in rich-MEA flow rate, the negative sign indicate transfer from liquid to vapour. The studies on CO_2 mass transfer rate and the heat transfer rate look at mass and heat transfer from the inner to outer radius of the RPB excluding the mass and heat transfer in the condenser and reboiler.

To further account for why there is an increase in the regeneration energy as shown in **Figures 5a,b,** the heat duty requirement in the reboiler is divided into three different parts: (i) Sensible heat to raise the temperature of the rich-MEA stream in the reboiler; (ii) Heat of reaction to reverse the absorption reaction and release CO_2; (iii) Heat of vapourisation to maintain the driving force for transfer of CO_2 from liquid phase to gas phase. **Figures 8a,b** and **9** show how the heat of vapourisation, sensible heat and the heat of reversible reaction increases with increase in rich-MEA flow rate respectively. **Figure 8a** shows that Heat of vapourisation is higher for high MEA concentration than lower MEA concentration this is due to the difference in their vapour composition (i.e. Case 1 has vapour composition of 0.25% H_2O, 97.13% MEA and Case 2 has 0.70% H_2O, 97.64% MEA and Case 3 has 1.49% H_2O, 97.85% MEA). Sensible heat for the three Cases is almost the same this is because the rich-MEA flow rate coming into the stripper is same and the specific heat capacity is relatively same and the difference in the specific heat capacity is counter balanced by the temperature differences. **Figure 9** shows that heat of reversible reaction increases with increase in concentration this is as a result more energy needed to break the CO_2 and MEA bonds and because of the decrease in the amount of free CO_2 as the MEA concentration increases. **Figure 10** shows how the reboiler duty requirement was divided for a fixed rich-MEA flowrate of 0.8 kg/s at three different MEA concentrations. This shows that the heat of reaction increases from 47%, to 65% and 74% when rich-MEA concentration increases from 32.9 wt%, to 50.443 wt% and 60.431 wt%. This is consistent with amount of CO_2 stripped as presented in Figure 4 (a).

Therefore, this study will help operators and designers of RPB regenerator to balance between energy consumption requirement and amount of CO_2 desorbed for a given Rich-MEA flow rate.

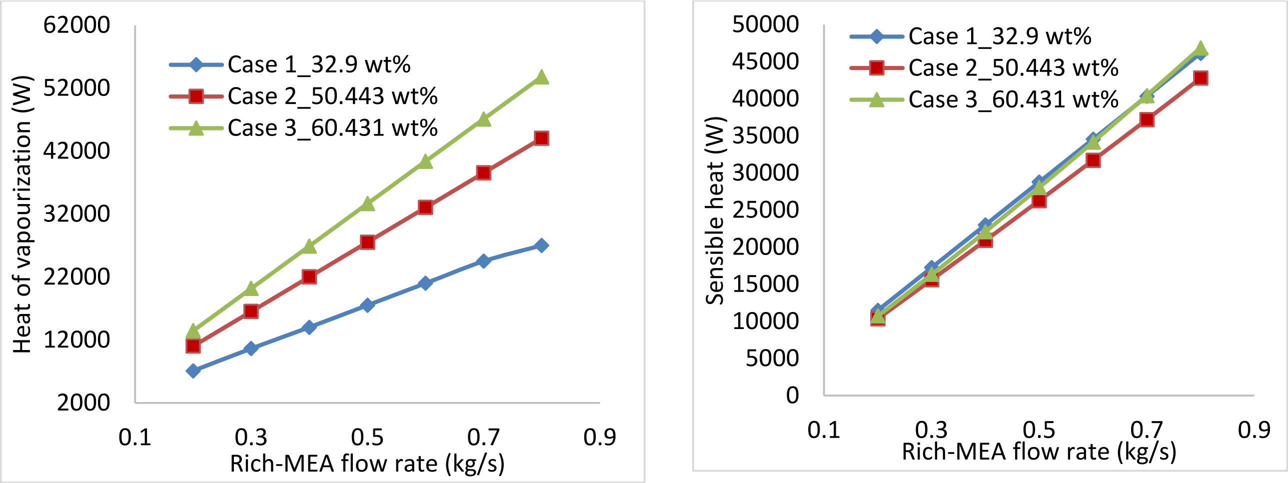

a

b

Figure 8 Effect of Rich-MEA flow rate on (a) Heat of vapourisation (b) Sensible heat

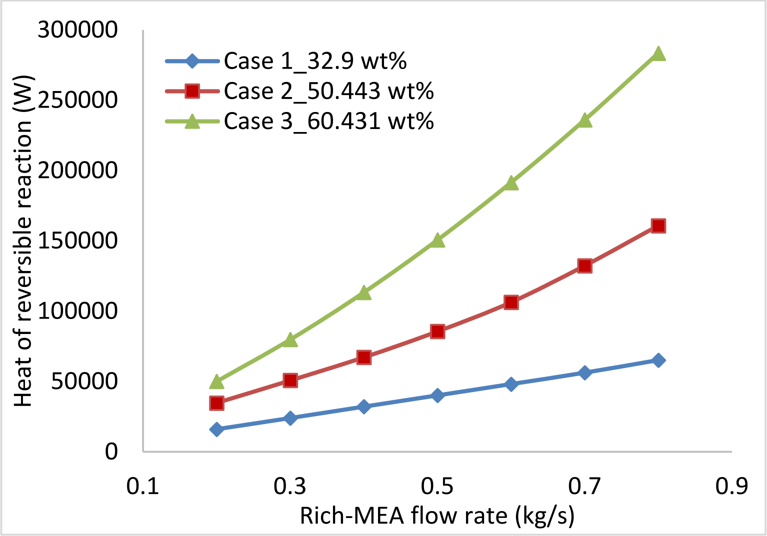

Figure 9 Effect of Rich-MEA flow rate on heat of reversible reaction

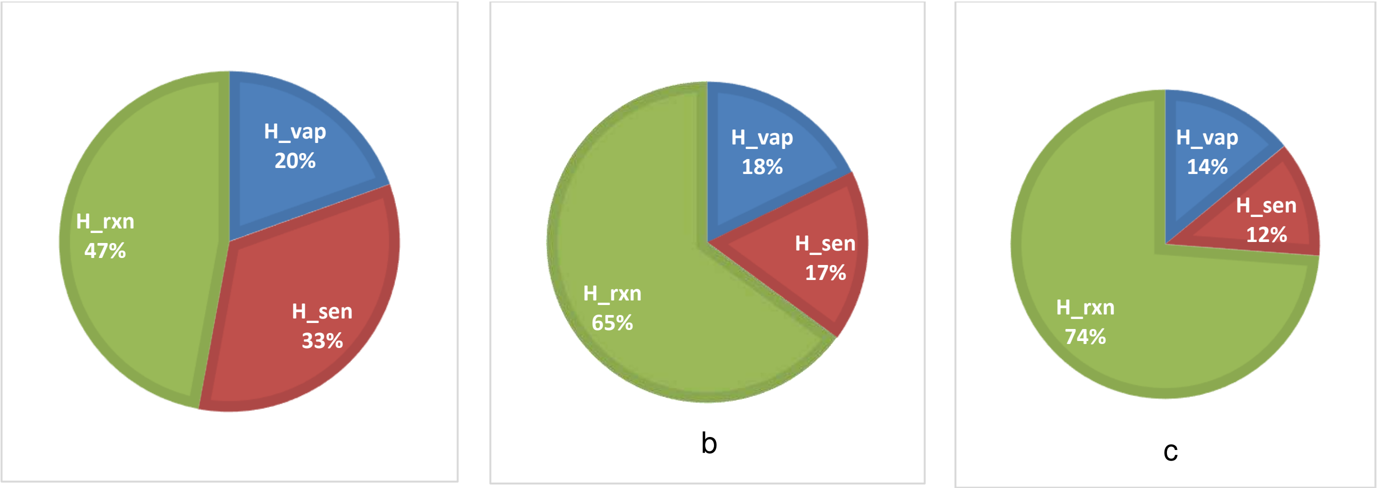

Figure 10 Heat contributions for 0.8 kg/s rich-MEA flowrate at different MEA concentration (a) 32.9 wt% MEA (b) 50.443 wt% MEA (c) 60.431 wt% MEA

4.2 *Effect of rotor speed on regeneration efficiency and regeneration energy*

4.2.1 Justification for case study

The higher the rotating speed of the intensified regenerator the higher the energy consumed, therefore it is important to understand the relationship that rotor speed has with rich-MEA solvent flow rate so that the energy requirement for driving the stripper can be reduced with respect to the amount of rich-MEA solvent regenerated.

4.2.2 Setup of the case study

For this study, the rotor speed was varied from 200 rpm and 1200 rpm in order to cover the experimental range of rotor speed reported in Jassim *et al* [24] and Cheng et al [25]. Input process conditions for this study are shown in **Table 9** (i.e. Cases 1 and 2). The reboiler temperature, rich-MEA flow rate and rich-MEA loading were kept constant at 120 °C 0.3 kg/s and 0.4823 mol/mol respectively for all the cases.

4.2.3 Results and discussion

Figure 11a shows that the regeneration efficiency increases with increase in the rotor speed. The impact of rotor speed on lean-MEA loading is shown in **Figure 11b**. Though higher rotor speed can produce opposite effect on mass and heat transfer by decreasing the residence time (as shown in **Figure 12a**) but this effect was counter balanced by the increase in the interfacial area which enhances mass and heat transfer. Burns *et al.* [46] stated that at higher rotor speed there are more of smaller liquid droplets and thinner liquid films in the packing regions of the bed, which means increase in interfacial area. The set-up in this study is different with the one reported in Section 4.1 where the lean-MEA loading was kept constant but in this study the recovery rate is kept constant for all the MEA concentrations, but the recovery rate changes as the rotor speed increases. **Figure 11a** shows that regeneration efficiency decreases with increase in concentration this is because the rich-MEA loading is maintained at same value and the recovery rate is fixed at the same value for different rotor speed meaning that the change between rich-MEA loading to lean-MEA loading is smaller for higher MEA concentration than lower MEA concentration. The amount of CO_2 desorbed from the stripper increases as the rotor speed increases as shown in **Figure 12b**. The amount of CO_2 desorbed for the two different cases are similar this is due to the model set-up where the recovery rate were maintained at the same value but varied with rotor speed.

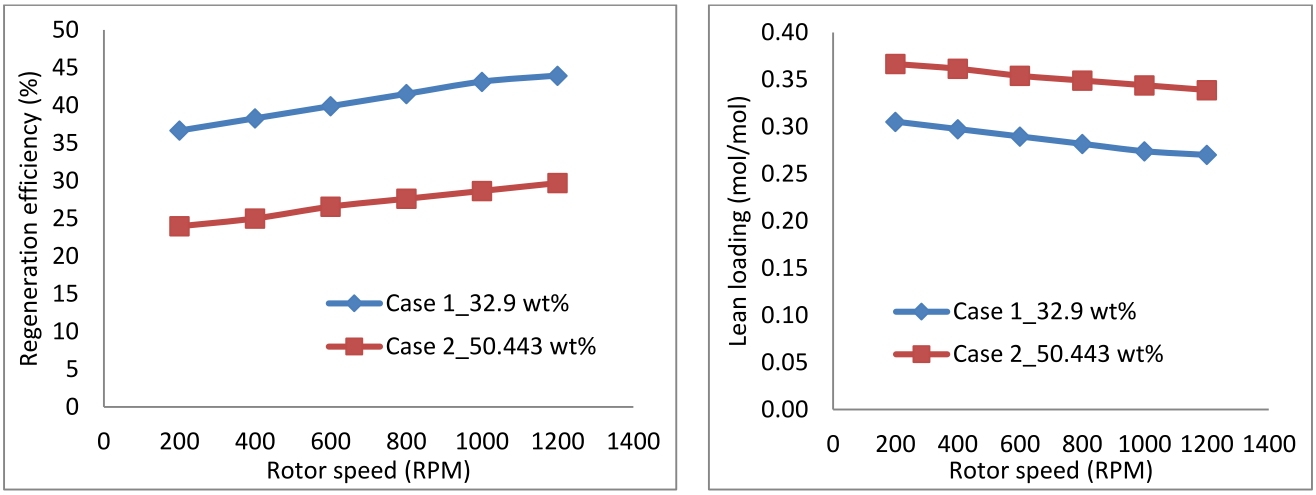

a b

Figure 11 Effect of rotor speed on (a) regeneration efficiency (b) lean loading

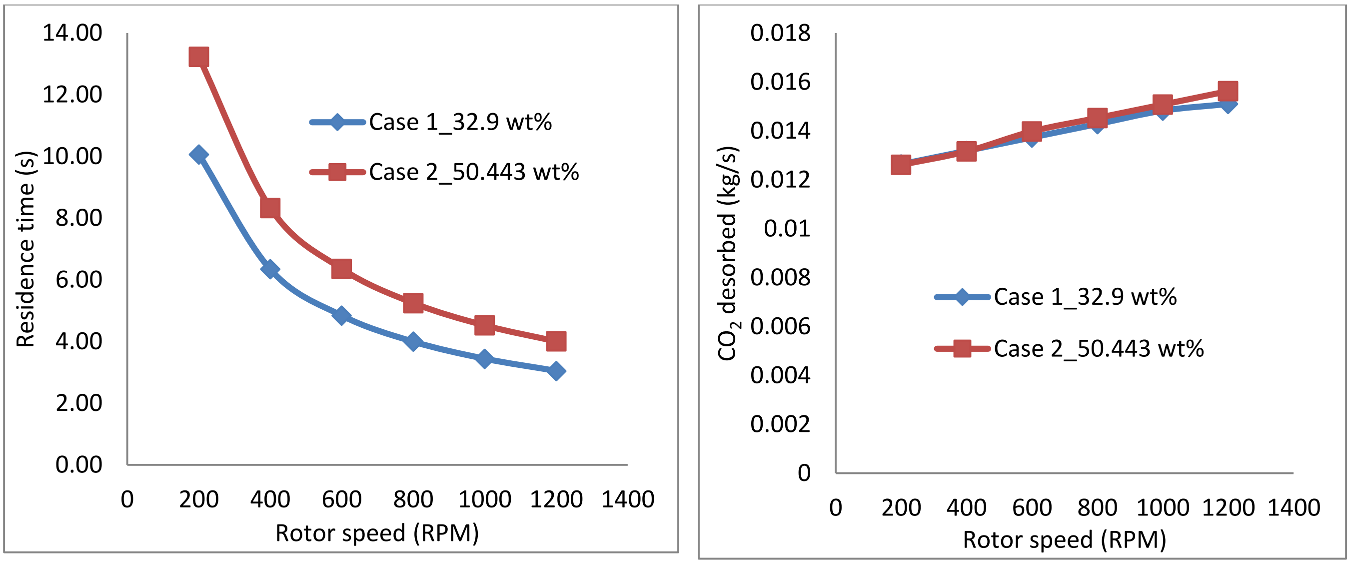

a b

Figure 12 Effect of rotor speed on (a) residence time (b) CO_2 desorbed

Increase in rotor speed decreases the regeneration energy as shown in **Figure 13a**. This is because increase in rotor speed leads to more liquid droplet and thin liquid films to dominate the packing resulting in increase in mass and heat transfer. Also at higher rotational speed the problem of liquid mal-distribution is overcome leading to higher wetted area which subsequently contributes to improving mass transfer. For all cases, the trend in **Figure 13a** (without motor energy) shows a drop in the regeneration energy as the rotor speed increases from 200 rpm to 1200 rpm this is because of increase in the rate of CO_2 stripped-off (**Figure 12b**). But when energy consumed by the motor is included **Figure 13b**, there is an increase in regeneration energy at rotor speed above 600 rpm for Case 2 and above 400 rpm for Case 1. This is because the motor energy is a function of square of rotor speed. Also **Figures 13a,b** shows that regeneration energy decreases with increase in MEA concentration this is due to smaller difference between rich-MEA loading and lean-loading as seen in **Figure 11b** (i.e. at rotor speed of 600rpm Cases 1 and 2 has lean-MEA loading as an output from the model of 0.2898 mol/mol and 0.354076 mol/mol respectively). The average percentage increase in regeneration energy when motor power is included is 6.44% and 6.84% for Case 1 and Case 2 respectively. **Figure 14** shows how the reboiler duty increases with increase in rotor speed. Case 1 has higher reboiler duty because the difference in rich-MEA to lean-MEA loading is bigger which means higher reboiler duty, since reboiler duty is related to the difference in lean and rich loading.

This study will help operator and designer of RPB regenerator in chosen the rotor speed that give lower regeneration energy without compromising the amount of CO_2 desorbed.

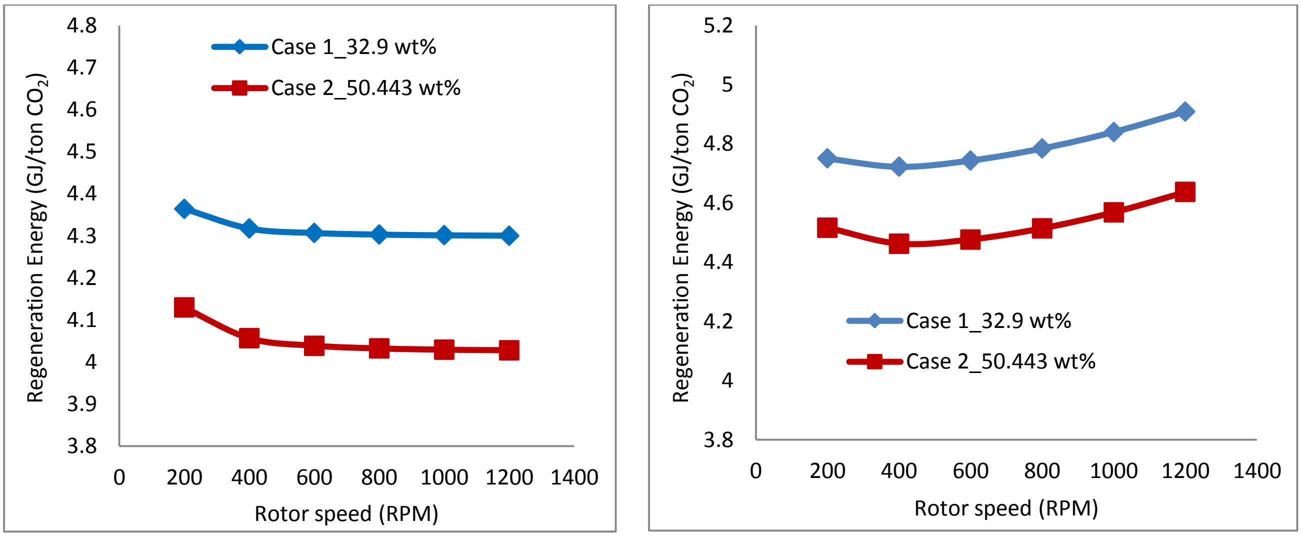

a b

Figure 13 Effect of rotor speed on regeneration energy (a) without motor energy (b) with motor energy

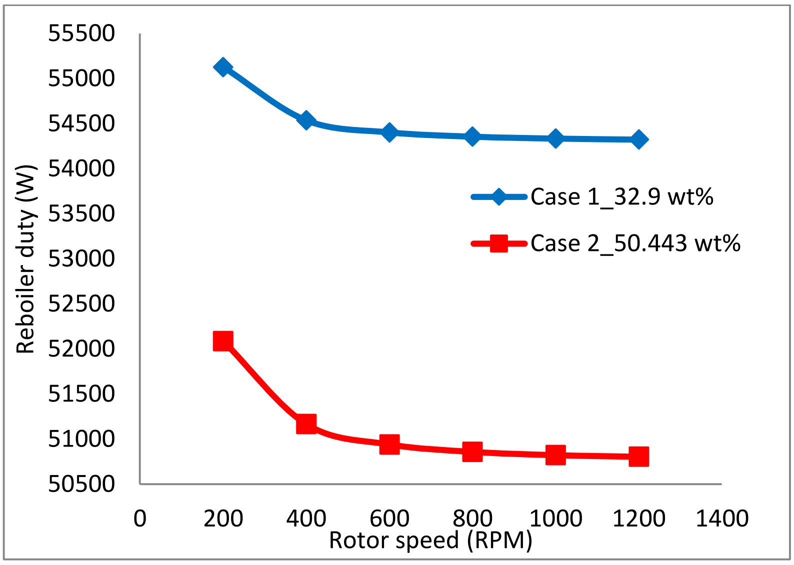

Figure 14 Effect of rotor speed on reboiler duty

4.3 *Effect of reboiler temperature on regeneration efficiency and energy*

4.3.1 Justification for case study

Operating intensified regenerator at the right reboiler temperature will lead to good system performance by reducing regeneration energy waste and also operating at relatively high regeneration efficiency.

4.3.2 Setup of the case study

For this study, the reboiler temperature was varied from 105 to 125 ^{o}C. Process input conditions are same as in **Table 9** (i.e. Cases 1 and 2). The rich-MEA flow rate and rich-MEA loading were kept constant at 0.3 kg/s and 0.4823 mol/mol respectively for all the cases.

4.3.3 Results and discussion

Figure 15a shows that the regeneration efficiency increases with increase in reboiler temperature. The percentage increase in regeneration efficiency as the reboiler temperature increases for Cases 1 and 2 is about the same 9.67% and 9.33% respectively. The model shows that regeneration efficiency for Case 1 which has lower MEA concentration is higher. This is due to lower lean-MEA loading coming out as shown in **Figure 15b** since at each reboiler temperature for Case 1 and 2, the amount CO_2 desorbed is maintained at around the same value and also more CO_2 was dissolved in higher MEA concentration than the lower MEA concentration in order to have the same rich-MEA loading coming into the stripper. **Figure 15b** shows that there is a decrease in lean-MEA loading as the reboiler temperature increases. This is because of increase in the amount of CO_2 stripped-off as shown in **Figure 16**.

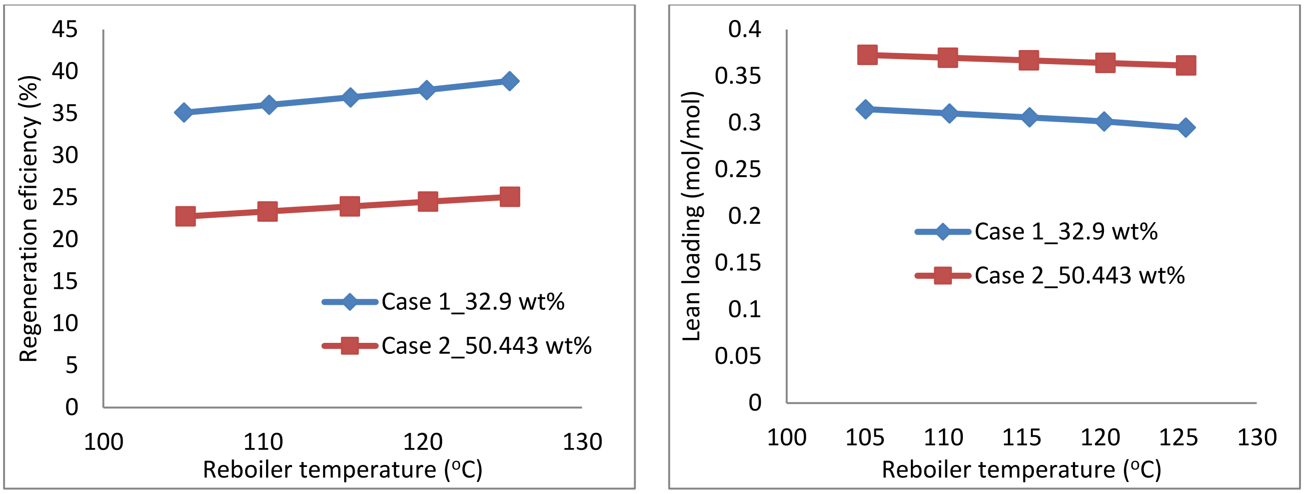

a

b

Figure 15 Effect of reboiler temperature on (a) regeneration efficiency (b) lean loading

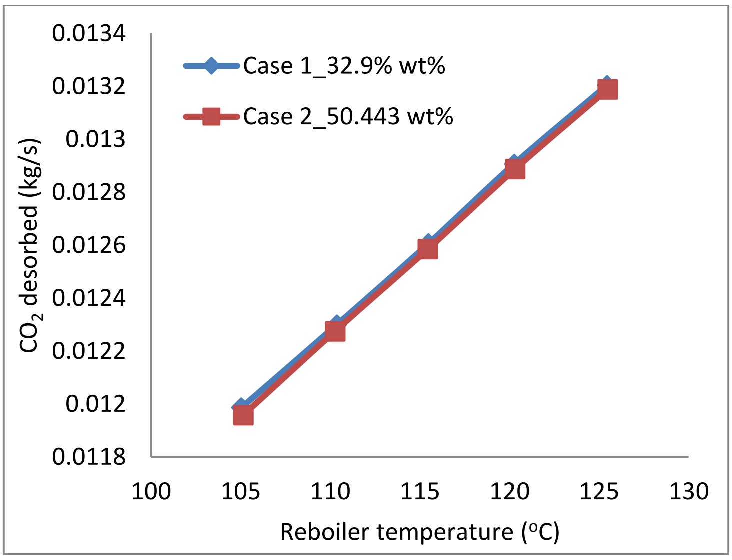

Figure 16 Effect of reboiler temperature on amount of CO_2 desorbed

There is a decrease and increase in regeneration energy as the reboiler temperature increases from 105 °C to 125 °C. From **Figure 16a,b** (with and without motor energy) the regeneration energy decreases as the reboiler temperature increases from 105 °C to 115 °C for Case 1 and 2, but this behaviour changes when the reboiler temperature exceed 115 °C. This is because at higher temperature we expect increase in water vapour flow rate which results in increase in regeneration energy because of heat of vaporisation of water. Also **Figure 19b** shows how the MEA composition in the vapour stream increases with increase in reboiler temperature this means increase in heat of vapourisation. Also from **Figure 15b** the loading different between the rich-MEA and lean-MEA stream is wide for Case 1 than Case 2 that is why it has higher reboiler duty requirement. **Figure 18** shows how the reboiler duty increases with increase in reboiler temperature. The decrease and increase in the regeneration energy can be further explained by **Figure 20 a,b** and **Figure 21** where the reboiler heat duty requirement is split into the heat of vapourisation, sensible heat and heat of reversible reaction. Increase in reboiler temperature leads to increase in heat of vapourisation and sensible heat while heat of reversible reaction decreases. The decrease in heat of reversible reaction is because of increase in rate of reaction as temperature increases.

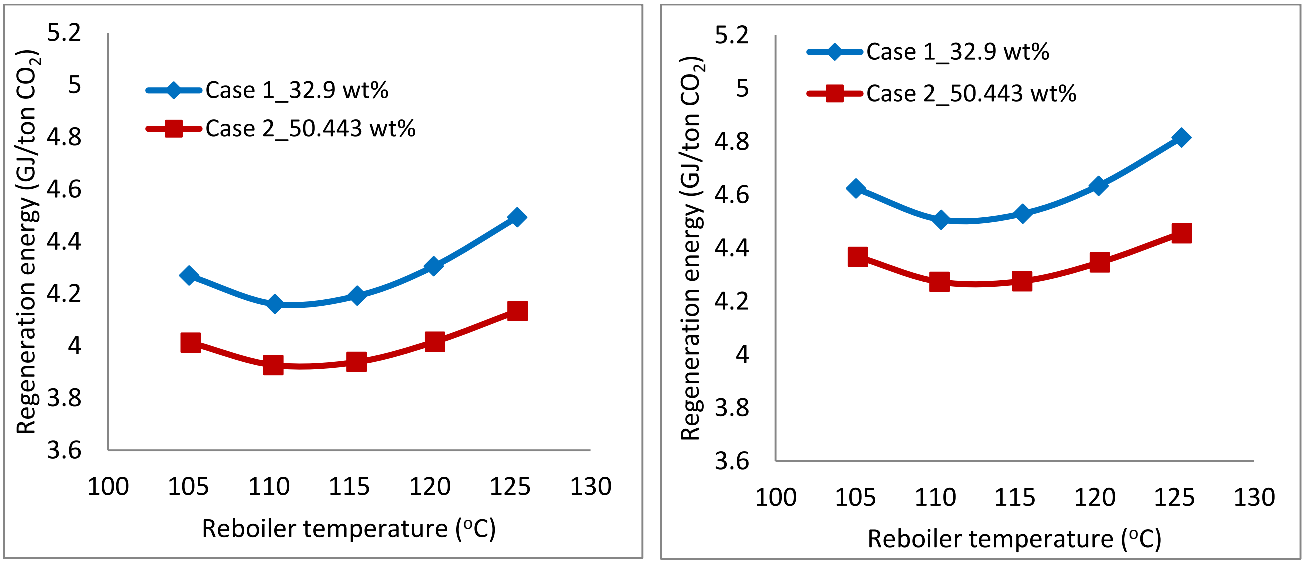

a b

Figure 17 Effect of reboiler temperature on regeneration energy (a) without motor energy (b) with motor energy

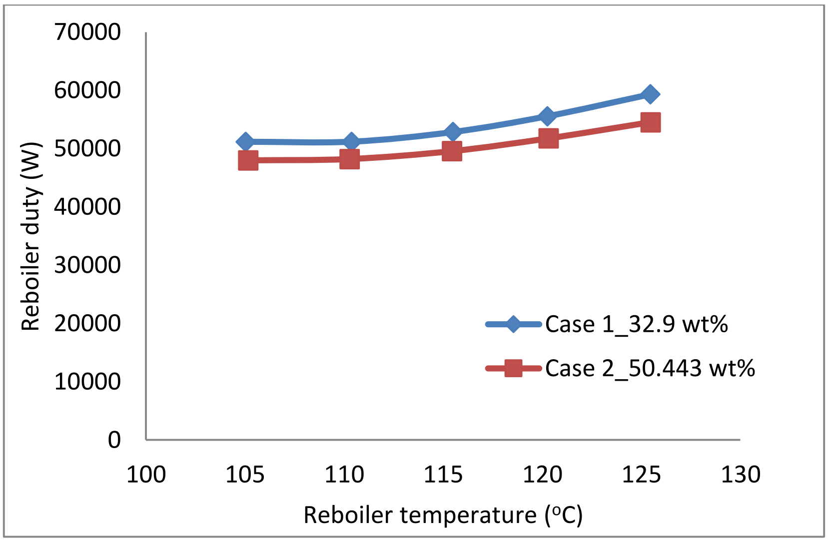

Figure 18 Effect of reboiler temperature on reboiler duty

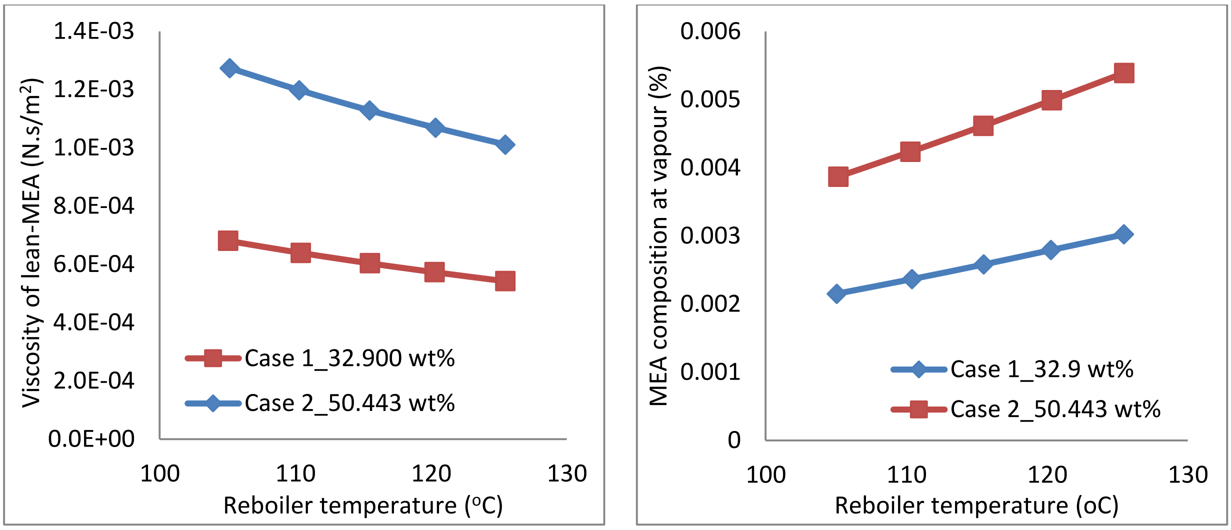

a b

Figure 19 Effect of reboiler temperature on (a) lean-MEA viscosity (b) MEA content in outlet vapour stream

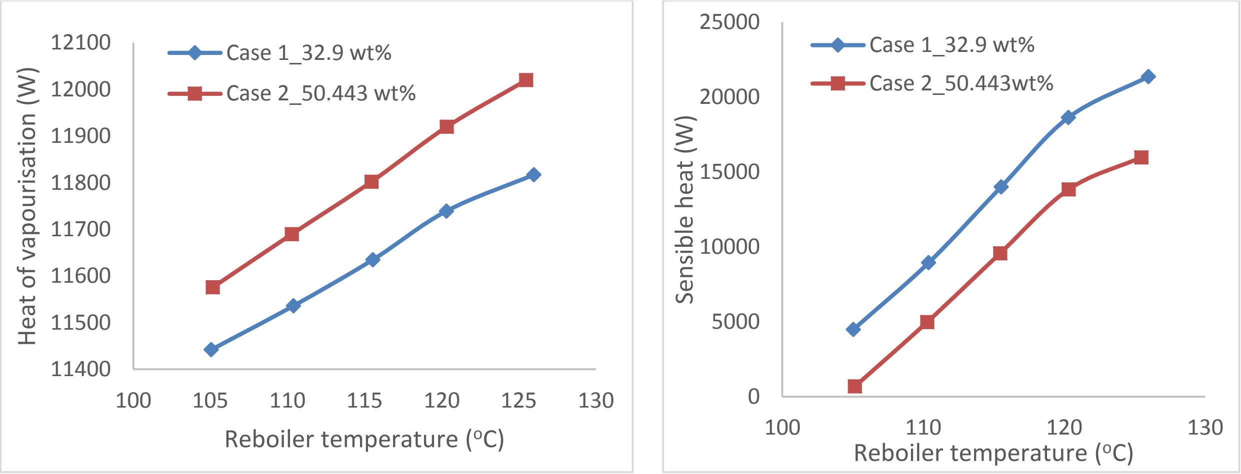

a b

Figure 20 Effect of reboiler temperature on (a) heat of vapourisation (b) sensible heat

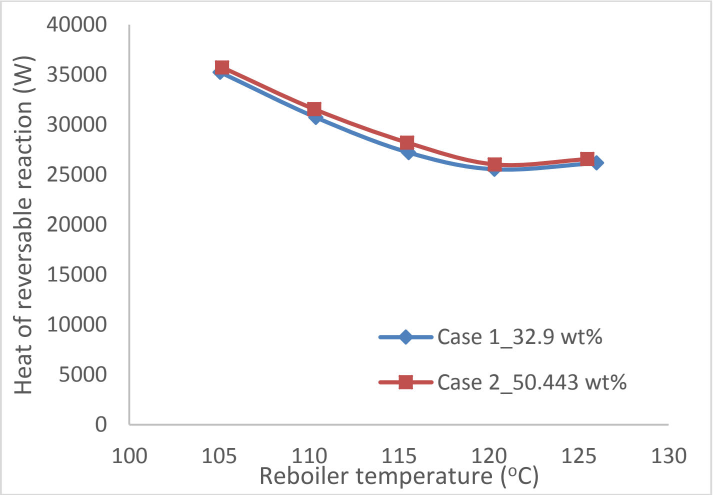

Figure 21 Effect of reboiler temperature on heat of reversible reaction

5 Comparison between RPB based intensified and PB based regenerator

5.1.1 Justification for the case study

This study was carried out to provide a comparison under some fixed conditions such as Rich-MEA flowrate, pressure, temperature, rich-MEA loading and lean-MEA loading between intensified regenerator and conventional regenerator.

5.1.2 Setup of the case study

For this study, **Table 10** presents the input conditions for the conventional and intensified regenerator. The rotor speed for the intensified regenerator is kept constant at 1000 rpm. Regeneration efficiency was kept constant at 37.16 % for both the conventional and the intensified regenerators.

Table 10 Process conditions for Conventional and RPB regenerator

Description	Conventional regenerator	RPB regenerator
	R-MEA	Lean-MEA
Rich-MEA temperature (^oC)	104	104
Rich-MEA pressure (kPa)	202.650	202.650
Rich-MEA flowrate (kg/s)	0.300	0.300
Rich-MEA loading (mol CO_2/mol MEA)	0.482	0.482
Mass-Fraction (wt%)		
H_2O	56.072	56.072
CO_2	11.328	11.328
MEA	32.600	32.600

5.1.3 Results and discussion

The results in Table 11 show a 44 times packing volume reduction in RPB regenerator compared to conventional PB regenerator without sumps. Using the assumption given by Agarwal *et al.* [23] that the casing volume of RPB is 4.5 times the rotating packing volume, the volume reduction compared to conventional PB regenerator is found to be 9.691 times smaller. The height of transfer unit (HTU) for conventional PB regenerator is calculated as 20.8 cm while for the RPB based intensified regenerator is 1.7 cm. The smaller HTU in RPB regenerator leads to its smaller size compared to conventional packed column. Wang *et al*. [20] performed preliminary technical and economic analysis for intensified PCC process compared with conventional PCC process. Initial prediction on the capital cost of the whole intensified PCC process can reduce by 1/6 (i.e. 16.7%) compared with the same capacity conventional PCC process. The 9.691 times reduction in the volume of intensified regenerator reported here confirmed to the possibility of having 16.7% cost reduction for intensified PCC process.

Table 11 Comparison between conventional and RPB stripper

Description	Conventional PB regenerator	RPB regenerator
Height of packing (m)	3.700	0.371 (r_o) 0.152 (r_i)
diameter (m)	0.476	0.167 axial depth
Packing Volume (m^3)	0.659	0.015
Packing volume reduction		43.933 times
Volume of unit (m^3)	0.659 [a]	0.068[b]
Volume reduction factor		9.691 times
Specific area (m^2/m^3)	151	2132
Void fraction	0.980	0.760
Lean-MEA loading (mol CO_2/mol MEA)	0.303	0.303

[a] Excluding sump

[b] Using the assumption given by Agarwal et al [23]

6 Conclusions

Intensified regenerator using RPB technology was modelled in this study. The steady state model was implemented by linking Aspen Plus® and visual FORTRAN. The model developed was validated with experimental data reported in Jassim *et al.* [24] and Cheng et al. [25]. The model validations show good agreement with the experimental data.

Process analysis on the effect of rich-MEA flow rate, rotational speed and reboiler temperature on CO_2 regeneration efficiency and regeneration energy were performed. For the given stripper (fixed in physical size), the study shows that an increase in the rich-MEA flow rate leads to an increase regeneration energy**.** There is an increase in the regeneration efficiency as the rotor speed increases but the regeneration energy decreases as the rotor speed increases since mass and heat transfer is enhanced at higher rotor speed. Reboiler temperature was varied from 105 °C to 125 °C, the results show a decrease in regeneration energy at reboiler temperature between 105 °C to 120 °C, but when the reboiler temperature exceeds 120 °C the regeneration energy begins to increase. Under the same process conditions, RPB based intensified stripper/regenerator has volume reduction of 9.691 times compared to conventional PB based stripper/regenerator. RPB stripper/regenerator shows great potential for application as a stripper and has much smaller size compared to conventional stripper which means reduction in capital cost.

Acknowledgement

The authors would like to acknowledge financial support from EPSRC Research Challenges in Carbon Capture for CCS (Ref: EP/M001458/2) and EU FP7 International Staff Research Exchange Scheme on power plant and carbon capture (Ref: PIRSES-GA-2013-612230).

References

[1] Department of Energy and Climate Change (DECC). Solid Fuels and Derived Gases Statistics: Data Sources and Methodologies. 2012;Available at: http://webarchive.nationalarchives.gov.uk/20121217150421/http://decc.gov.uk/en/content/cms/statistics/energy_stats/source/electricity/electricity.aspx; (accessed May,2013).

[2] Albo J, Luis P, Irabien A. Carbon dioxide capture from flue gases using a cross-flow membrane contactor and the ionic liquid 1-ethyl-3-methylimidazolium ethylsulfate. Ind Eng Chem Res 2010;49:11045-51.

[3] CO2-Earth. Daily CO_2: Mauna Loa Observatory/ Atmospheric CO_2 Concentration
. Available at: https://www co2 earth/daily-co2 (accessed April, 2017).

[4] World Meteorological Organization (WMO). Press Release No. 991
. 26 May 2014;http://www.wmo.int/pages/mediacentre/press_releases/pr_991_en.html (accessed June, 2014).

[5] Intergovernmental Panel on Climate Change (IPCC). Contribution of Working Group III to the Fourth Assessment Report of the Intergovernmental Panel on Climate Change. Cambridge, United Kingdom/New York, United States: Cambridge University Press, 2007.

[6] International Energy Agency. Carbon Capture and Storage Model Regulatory Framework. IEA 2010;Available at: http://www.iea.org/publications/freepublications/publication/model_framework.pdf, (accessed May 2013).

[7] MacDowell N, Florin N, Buchard A, Hallett J, Galindo A, Jackson G et al. An overview of CO_2 capture technologies. Energy & Environmental Science 2010;3:1645-69.

[8] Dugas RE. Pilot plant study of carbon dioxide capture by aqueous monoethanolamine. MSE Thesis, University of Texas at Austin 2006.

[9] Lawal A, Wang M, Stephenson P, Obi O. Demonstrating full-scale post-combustion CO_2 capture for coal-fired power plants through dynamic modelling and simulation. Fuel 2012;101:115-28.

[10] Lawal A, Wang M, Stephenson P, Koumpouras G, Yeung H. Dynamic modelling and analysis of post-combustion CO_2 chemical absorption process for coal-fired power plants. Fuel 2010;89:2791-801.

[11] Lawal A, Wang M, Stephenson P, Yeung H. Dynamic Modeling and Simulation of CO_2 Chemical Absorption Process for Coal-Fired Power Plants. Computer Aided Chemical Engineering 2009;27:1725-30.

[12] Li K, Leigh W, Feron P, Yu H, Tade M. Systematic study of aqueous monoethanolamine (MEA)-based CO2 capture process: Techno-economic assessment of the MEA process and its improvements. Appl Energy 2016;165:648-59.

[13] Oh S, Binns M, Cho H, Kim J. Energy minimization of MEA-based CO2 capture process. Appl Energy 2016;169:353-62.

[14] Sharifzadeh M, Bumb P, Shah N. Carbon capture from pulverized coal power plant (PCPP): Solvent performance comparison at an industrial scale. Appl Energy 2016;163:423-35.

[15] Hanak DP, Biliyok C, Manovic V. Efficiency improvements for the coal-fired power plant retrofit with CO2 capture plant using chilled ammonia process. Appl Energy 2015;151:258-72.

[16] Zhao B, Liu F, Cui Z, Liu C, Yue H, Tang S et al. Enhancing the energetic efficiency of MDEA/PZ-based CO2 capture technology for a 650 MW power plant: Process improvement. Appl Energy 2017;185, Part 1:362-75.

[17] Kvamsdal H, Jakobsen J, Hoff K. Dynamic modeling and simulation of a CO_2 absorber column for post-combustion CO_2 capture. Chemical Engineering and Processing: Process Intensification 2009;48:135-44.

[18] Reay D. The role of process intensification in cutting greenhouse gas emissions. Appl Therm Eng 2008;28:2011-9.

[19] Wang M, Lawal A, Stephenson P, Sidders J, Ramshaw C. Post-combustion CO_2 capture with chemical absorption: A state-of-the-art review. Chem Eng Res Design 2011;89:1609-24.

[20] Wang M, Joel AS, Ramshaw C, Eimer D, Musa NM. Process intensification for post-combustion CO2 capture with chemical absorption: A critical review. Appl Energy 2015;158:275-91.

[21] Joel AS, Wang M, Ramshaw C, Oko E. Process analysis of intensified absorber for post-combustion CO_2 capture through modelling and simulation. International Journal of Greenhouse Gas Control 2014;21:91-100.

[22] Joel AS, Wang M, Ramshaw C. Modelling and simulation of intensified absorber for post-combustion CO_2 capture using different mass transfer correlations. Appl Therm Eng 2015;74:47-53.

[23] Agarwal L, Pavani V, Rao D, Kaistha N. Process intensification in HiGee absorption and distillation: design procedure and applications. Ind Eng Chem Res 2010;49:10046-58.

[24] Jassim MS, Rochelle G, Eimer D, Ramshaw C. Carbon dioxide absorption and desorption in aqueous monoethanolamine solutions in a rotating packed bed. Ind Eng Chem Res 2007;46:2823-33.

[25] Cheng H, Lai C, Tan C. Thermal regeneration of alkanolamine solutions in a rotating packed bed. International Journal of Greenhouse Gas Control 2013;16:206-16.

[26] Zhao B, Su Y, Tao W. Mass transfer performance of CO_2 capture in rotating packed bed: Dimensionless modeling and intelligent prediction. Appl Energy 2014;136:132-42.

[27] Chamchan N, Chang J, Hsu H, Kang J, Wong DSH, Jang S et al. Comparison of rotating packed bed and packed bed absorber in pilot plant and model simulation for CO2 capture. Journal of the Taiwan Institute of Chemical Engineers 2017;73:20-6.

[28] Lin C, Lin Y, Tan C. Evaluation of alkanolamine solutions for carbon dioxide removal in cross-flow rotating packed beds. J Hazard Mater 2010;175:344-51.

[29] Wang G, Xu Z, Yu Y, Ji J. Performance of a rotating zigzag bed—A new HIGEE. Chemical Engineering and Processing: Process Intensification 2008;47:2131-9.

[30] BERR. Advanced power plant using high efficiency boiler/turbine. Report BPB010. BERR, Department for Business Enterprise and Regulatory Reform. 2006;Available at: http://webarchive.nationalarchives.gov.uk/20090609003228/http://www.berr.gov.uk/files/file30703.pdf (accessed August 2015).

[31] Kothandaraman A, Nord L, Bolland O, Herzog HJ, McRae GJ. Comparison of solvents for post-combustion capture of CO_2 by chemical absorption. Energy Procedia 2009;1:1373-80.

[32] Chen Y, Lin F, Lin C, Tai CY, Liu H. Packing characteristics for mass transfer in a rotating packed bed. Ind Eng Chem Res 2006;45:6846-53.

[33] Chen Y. Correlations of mass transfer coefficients in a rotating packed bed. Ind Eng Chem Res 2011;50:1778-85.

[34] Luo Y, Chu G, Zou H, Zhao Z, Dudukovic MP, Chen J. Gas–liquid effective interfacial area in a rotating packed bed. Ind Eng Chem Res 2012;51:16320-5.

[35] Burns J, Jamil J, Ramshaw C. Process intensification: operating characteristics of rotating packed beds—determination of liquid hold-up for a high-voidage structured packing. Chemical Engineering Science 2000;55:2401-15.

[36] Llerena-Chavez H, Larachi F. Analysis of flow in rotating packed beds via CFD simulations—Dry pressure drop and gas flow maldistribution. Chemical Engineering Science 2009;64:2113-26.

[37] Kang J, Sun K, Wong DS, Jang S, Tan C. Modeling studies on absorption of CO2 by monoethanolamine in rotating packed bed. International Journal of Greenhouse Gas Control 2014;25:141-50.

[38] AspenTech. Aspen Physical Properties System – Physical Property Methods. 2010, Available at: http://support.aspentech.com/ (accessed May 2014).

[39] Zhang Y, Chen C. Modeling CO 2 Absorption and Desorption by Aqueous Monoethanolamine Solution with Aspen Rate-based Model. Energy Procedia 2013;37:1584-96.

[40] Tung H, Mah RS. Modeling liquid mass transfer in higee separation process. Chem Eng Commun 1985;39:147-53.

[41] Onda K, Sada E, Takeuchi H. Gas absorption with chemical reaction in packed columns. J Chem Eng Japan 1968;1:62-6.

[42] Sandilya P, Rao D, Sharma A, Biswas G. Gas-phase mass transfer in a centrifugal contactor. Ind Eng Chem Res 2001;40:384-92.

[43] Singh SP, Wilson JH, Counce RM, Lucero AJ, Reed GD, Ashworth RA et al. Removal of volatile organic compounds from groundwater using a rotary air stripper. Ind Eng Chem Res 1992;31:574-80.

[44] Jassim MS. Process intensification: absorption and desorption of carbon dioxide from monoethanolamine solutions using Higee technology. Newcastle University, UK (PhD Thesis) 2002.

[45] Chambers H, Wall M. Some factors affecting the design of centrifugal gas absorbers. Trans.Inst.Chem.Eng 1954;32:S96-S107.

[46] Burns J, Ramshaw C. Process intensification: visual study of liquid maldistribution in rotating packed beds. Chemical Engineering Science 1996;51:1347-52.